

 Open access • Posted Content • DOI:10.1101/2020.02.04.932376

## **PRX1, PRX44, and PRX73 are Class-III extensin-related peroxidases that modulates root hair growth in *Arabidopsis thaliana*** — [Source link](#)

Eliana Marzol, Cecilia Borassi, José M. Estevez

**Institutions:** Andrés Bello National University, Fundación Instituto Leloir

**Published on:** 04 Feb 2020 - bioRxiv (Cold Spring Harbor Laboratory)

**Topics:** Root hair and Extensin

Related papers:

- [The class III peroxidase PRX17 is a direct target of the MADS-box transcription factor AGAMOUS-LIKE15 \(AGL15\) and participates in lignified tissue formation](#)
- [Roles of cell wall peroxidases in plant development](#)
- [Cell wall-associated ROOT HAIR SPECIFIC 10, a proline-rich receptor-like kinase, is a negative modulator of Arabidopsis root hair growth](#)
- [ROOT HAIR DEFECTIVE SIX-LIKE4 \(RSL4\) promotes root hair elongation by transcriptionally regulating the expression of genes required for cell growth](#)
- [S-nitrosoglutathione promotes cell wall remodelling, alters the transcriptional profile and induces root hair formation in the hairless root hair defective 6 \(rhd6\) mutant of Arabidopsis thaliana](#)

Share this paper:    

View more about this paper here: <https://typeset.io/papers/prx1-prx44-and-prx73-are-class-iii-extensin-related-1a28z3dqu1>

1 **Running Head:** PRX01, PRX44 and PRX73 are peroxidases active in root hair growth

2

3 **Authors for Correspondence:**

4 *José M. Estevez*

5 Fundación Instituto Leloir, Av. Patricias Argentinas 435, Buenos Aires C1405BWE, Argentina. TE: 54-  
6 115238-7500 EXT. 3206

7 Centro de Biotecnología Vegetal, Facultad de Ciencias de la Vida, Universidad Andrés Bello and  
8 Millennium Institute for Integrative Biology (iBio), Santiago CP 8370146, Chile.

9 Email: [jestevez@leloir.org.ar](mailto:jestevez@leloir.org.ar) / [jose.estevez@unab.cl](mailto:jose.estevez@unab.cl)

10

11

12 **Research area most appropriate for paper:** Plant Biology

13

14

15 Text Word count: 6,668

16 Figures 1-4

17 Table 1

18 Experimental procedures

19 References: 74

20

## RAPID REPORT

### 21 **Class III peroxidases PRX01, PRX44, and PRX73 potentially target extensins during root hair** 22 **growth in *Arabidopsis thaliana***

23

24 Eliana Marzol<sup>1,#</sup>, Cecilia Borassi<sup>1,#</sup>, Philippe Ranocha<sup>2</sup>, Ariel. A. Aptekman<sup>3,4</sup>, Mauro Bringas<sup>5</sup>, Janice  
25 Pennington<sup>6</sup>, Julio Paez-Valencia<sup>6</sup>, Javier Martínez Pacheco<sup>1</sup>, Diana Rosa Rodríguez García<sup>1</sup>,  
26 Yossmayer del Carmen Rondón Guerrero<sup>1</sup>, Mariana Carignani<sup>1</sup>, Silvina Mangano<sup>1</sup>, Margaret  
27 Fleming<sup>7</sup>, John W. Mishler-Elmore<sup>8</sup>, Francisca Blanco-Herrera<sup>9,10</sup>, Patricia Bedinger<sup>7</sup>, Christophe  
28 Dunand<sup>2</sup>, Luciana Capece<sup>5</sup>, Alejandro D. Nadra<sup>3,4</sup>, Michael Held<sup>8</sup>, Marisa S. Otegui<sup>6,11</sup> & José M.  
29 Estevez<sup>1,9,†</sup>

30

31 <sup>1</sup>Fundación Instituto Leloir and IIBBA-CONICET. Av. Patricias Argentinas 435, Buenos Aires C1405BWE,  
32 Argentina.

33 <sup>2</sup>Université de Toulouse, UPS, UMR 5546, Laboratoire de Recherche en Sciences Végétales, F-31326  
34 CNRS, UMR 5546 Castanet-Tolosan, France.

35 <sup>3</sup>Departamento de Fisiología, Biología Molecular y Celular, Instituto de Biociencias, Biotecnología y  
36 Biología Traslacional (iB3). Facultad de Ciencias Exactas y Naturales, Universidad de Buenos Aires,  
37 Ciudad Universitaria, Buenos Aires C1428EGA, Argentina.

38 <sup>4</sup>Departamento de Química Biológica, Facultad de Ciencias Exactas y Naturales, Universidad de  
39 Buenos Aires (IQUIBICEN-CONICET), Ciudad Universitaria, Buenos Aires C1428EGA, Argentina.

40 <sup>5</sup>Departamento de Química Inorgánica, Analítica y Química Física, Facultad de Ciencias Exactas y  
41 Naturales, Universidad de Buenos Aires (INQUIMAE-CONICET), Buenos Aires, CP. C1428EGA,  
42 Argentina.

43 <sup>6</sup>Laboratory of Cell and Molecular Biology, University of Wisconsin, Madison, WI, USA.

44 <sup>7</sup>Department of Biology, Colorado State University, Fort Collins, Colorado 80523-1878, USA.

45 <sup>8</sup>Department of Chemistry and Biochemistry, Ohio University, Athens, OH 45701, USA.

46 <sup>9</sup>Centro de Biotecnología Vegetal, Facultad de Ciencias de la Vida, Universidad Andrés Bello and  
47 Millennium Institute for Integrative Biology (iBio), Santiago, Chile.

48 <sup>10</sup>Center of Applied Ecology and Sustainability (CAPES), Chile.

49 <sup>11</sup>Departments of Botany and Genetics, University of Wisconsin, Madison, WI, USA.

50

51 #co-first authors

52 † Correspondence should be addressed. Email: [jestevez@leloir.org.ar](mailto:jestevez@leloir.org.ar) / [jose.estevez@unab.cl](mailto:jose.estevez@unab.cl) (J.M.E).

53

54 Key words: Arabidopsis, cell walls, extensins, root hairs, ROS, class-III peroxidases.

55

56 Word count: 4,295

57 **Abstract**

58

59 • Root hair cells are important sensors of soil conditions. Expanding several hundred times their  
60 original size, root hairs grow towards and absorb water-soluble nutrients. This rapid growth is  
61 oscillatory and is mediated by continuous remodelling of the cell wall. Root hair cell walls contain  
62 polysaccharides and hydroxyproline-rich glycoproteins including extensins (EXTs).

63

64 • Class-III peroxidases (PRXs) are secreted into the apoplastic space and are thought to trigger either  
65 cell wall loosening, mediated by oxygen radical species, or polymerization of cell wall components,  
66 including the Tyr-mediated assembly of EXT networks (EXT-PRXs). The precise role of these EXT-  
67 PRXs is unknown.

68

69 • Using genetic, biochemical, and modeling approaches, we identified and characterized three root  
70 hair-specific putative EXT-PRXs, PRX01, PRX44, and PRX73. The triple mutant *prx01,44,73* and the  
71 PRX44 and PRX73 overexpressors had opposite phenotypes with respect to root hair growth,  
72 peroxidase activity and ROS production with a clear impact on cell wall thickness.

73

74 • Modeling and docking calculations suggested that these three putative EXT-PRXs may interact with  
75 non-*O*-glycosylated sections of EXT peptides that reduce the Tyr-to-Tyr intra-chain distances in EXT  
76 aggregates and thereby may enhance Tyr crosslinking. These results suggest that these three  
77 putative EXT-PRXs control cell wall properties during the polar expansion of root hair cells.

78

79 Word count: 200

## 80 Introduction

81 Primary cell walls, composed by a diverse network containing mainly polysaccharides and a small  
82 amount of structural glycoproteins, regulate cell elongation, which is crucial for several plant growth  
83 and developmental processes. Extensins (EXTs) belong to hydroxyproline (Hyp)-rich glycoprotein  
84 (HRGP) superfamily and broadly include related glycoproteins such as proline-rich proteins (PRPs) and  
85 leucine-rich repeat extensins (LRXs) with multiple Ser-(Pro)<sub>3-5</sub> repeats that may be *O*-glycosylated and  
86 contain Tyr (Y)-based motifs (Lamport et al. 2011; Marzol et al. 2018). EXTs require several  
87 modifications before they become functional (Lamport et al., 2011; Marzol et al. 2018). After being  
88 hydroxylated and *O*-glycosylated in the secretory pathway, the secreted *O*-glycosylated EXTs are  
89 crosslinked and insolubilized in the plant cell wall by the oxidative activity of secreted class-III  
90 peroxidases (PRXs) on the Tyr-based motifs (Baumberger 2001, 2003; Ringli 2010; Held et al. 2004;  
91 Lamport et al., 2011; Chen et al. 2015; Marzol et al. 2018). PRXs are thought to facilitate both intra  
92 and inter-molecular covalent Tyr–Tyr crosslinks in EXT networks, possibly through the assembly of  
93 triple helices (Velasquez et al. 2015a; Marzol et al. 2018) by generating *isodityrosine* units (IDT) and  
94 *pulcherosine*, or *di-isodityrosine* (Di-IDT), respectively (Brady et al., 1996; 1998; Held et al. 2004). In  
95 addition, *O*-glycosylation levels in EXTs also affect their insolubilization process in the cell wall (Chen  
96 et al. 2015; Velasquez et al. 2015a) since it might influence the EXT interactions with other cell wall  
97 components (Nuñez et al., 2009; Valentin et al., 2010). However, the underlying molecular  
98 mechanisms of EXT crosslinking and assembly have not been fully determined. It is proposed that *O*-  
99 glycosylation levels as well as the presence of Tyr-mediated crosslinking in EXT and related  
100 glycoproteins allow them to form a dendritic glycoprotein network in the cell wall. This EXT network  
101 affects *de novo* cell wall formation during embryo development (Hall and Cannon 2002; Cannon *et al.*,  
102 2008), they are also implicated in roots, petioles and rosette leaves growth (Saito et al 2014; Møller  
103 et al. 2017) and in polar cell expansion processes in root hairs (Baumberger 2001, 2003; Ringli 2010;  
104 Velasquez et al. 2011; 2012; 2015a,b) as well as in pollen tubes (Fabrice et al. 2018; Sede et al. 2018;  
105 Wang et al. 2018).

106  
107 Apoplastic class-III PRXs are heme-iron-dependent proteins, members of a large multigenic family in  
108 land plants, with 73 members in *Arabidopsis thaliana* (Passardi et al. 2004; Weng and Chapple, 2010).  
109 These PRXs catalyze several different classes of reactions. PRX activities coupled to *apo*ROS molecules  
110 (*apo*H<sub>2</sub>O<sub>2</sub>) directly affect the degree of cell wall crosslinking (Dunand et al. 2007) by oxidizing cell wall  
111 compounds and leading to stiffening of the cell wall through a peroxidative cycle (PC) (Passardi et al.  
112 2004, Cosio & Dunand 2009; Lamport et al. 2011). By contrast, *apo*ROS coupled to PRX activity  
113 enhances non-enzymatic cell wall-loosening by producing oxygen radical species (e.g., •OH) and  
114 promoting growth in the hydroxylic cycle (HC). In this HC cycle, PRXs catalyze the reaction in which  
115 hydroxyl radicals (•OH) are produced from H<sub>2</sub>O<sub>2</sub> after O<sub>2</sub>•<sup>-</sup> dismutation. In this manner, some PRXs  
116 (e.g. PRX36) may function in weaken plant cell walls by the generated •OH that cleave cell wall  
117 polysaccharides in seed mucilage extrusion in epidermal cells in the *Arabidopsis* seed coat (Kunieda

118 et al., 2013). It is unclear how these opposite effects on cell wall polymers are coordinated during  
119 plant growth (Passardi et al. 2004, Cosio & Dunand 2009; Lee et al. 2013; Ropollo et al. 2011; Lee et  
120 al 2018; Francoz et al. 2019). Finally, PRXs also contribute to the superoxide radical ( $O_2^{\bullet-}$ ) pool by  
121 oxidizing singlet oxygen in the oxidative cycle (OC), thereby affecting  $_{apo}H_2O_2$  levels. Thus, several PRXs  
122 are involved in the oxidative polymerization of monolignols in the apoplast of the lignifying cells in  
123 xylem (e.g. PRX017, Cosio et al 2017; PRX72, Herrero et al. 2013), in the root endodermis (e.g. PRX64;  
124 Lee et al. 2013; Ropollo et al. 2011), and in petal detachment (Lee et al 2018). In addition, PRXs are  
125 able to polymerize other components of the plant cell wall such as suberin (Bernards et al., 1999),  
126 pectins (Francoz et al. 2019), and EXTs (Schnabelrauch *et al.*, 1996; Jackson et al., 2001). Although  
127 several candidates of PRXs have been associated specifically with EXT-crosslinking (EXT-PRXs) by *in*  
128 *vitro* studies (Schnabelrauch et al., 1996; Wojtaszek et al., 1997; Jackson et al., 2001; Price et al., 2003;  
129 Pereira et al. 2011; Dong et al., 2015) or based on an immunolabelling extensin study linked to a  
130 genetic profile (Jacobowitz et al. 2019), the *in vivo* characterization and mode of action of these EXT-  
131 PRXs remain largely unknown. In this work, we used a combination of reverse genetics, molecular and  
132 cell biology, computational molecular modeling, and biochemistry to identify three apoplastic PRXs,  
133 PRX01, PRX44 and PRX73, as key enzymes possibly potentially involved in Tyr-crosslinking of cell wall  
134 EXTs in growing root hair cells. In addition, we propose a hypothetical model in which O-glycosylation  
135 levels on the triple helixes of EXTs might regulate the degree of Tyr-crosslinking affecting the  
136 expansion properties of cell walls as suggested before based on the extended helical polyproline-II  
137 conformation state of EXTs (Stafstrom & Staehelin 1986; Owen et al., 2010; Ishiwata et al., 2014)  
138 together with an experimental Atomic Force Microscopic (AFM) analysis of crosslinked EXT3  
139 monomers (Cannon et al. 2008) linked to modelling approaches (Velasquez et al. 2015a; Marzol et al  
140 2018). Our results open the way for the discovery of similar interactions in EXT assemblies during root  
141 hair development and in response to the environmental changes, such fluctuating nutrient availability  
142 in the soil.

143

## 144 **Results and Discussion**

145 In this work, we have chosen to analyze root hair cells because they are an excellent model for tracking  
146 cell elongation and identifying PRXs involved in EXT assembly. In previous work, the phenotypes of  
147 mutants for PRX01, PRX44 and PRX73 suggested that these PRXs are involved in root hair growth and  
148 ROS homeostasis, although their mechanisms of action remained to be characterized (Mangano et al.  
149 2017). All three PRXs are under the transcriptional regulation of the root hair specific transcription  
150 factor RSL4 (Yi et al. 2010; Mangano et al. 2017). As expected, these three PRXs are also highly co-  
151 expressed with other root hair-specific genes encoding cell wall EXTs (e.g., EXT6-7, EXT12-14, and  
152 EXT18) and EXT-related glycoproteins (e.g. LRX1 and LRX2), which functions in cell expansion (Ringli  
153 2010; Velasquez et al. 2011; Velasquez et al. 2015b) (**Figure S1**). Based on this evidence, we  
154 hypothesized that these three PRXs might be EXT-PRXs and catalyze Tyr-crosslinks to assemble EXTs  
155 in root hair cell walls.

156  
157 To validate that PRX01, PRX44, and PRX73 are expressed specifically in root hairs, we made  
158 transcriptional reporters harboring GFP-tagged fusions of the promoter regions of their genes. In  
159 agreement with the *in silico* database (Mangano et al. 2017 and **Figure S1**), all three genes were  
160 strongly expressed in root hair cells during cell elongation (**Figure 1A**). Single mutants for these three  
161 PRXs showed almost normal root hair growth (Mangano et al. 2017), suggesting a high degree of  
162 functional redundancy. Double combinations of *prx44 prx73* (Mangano et al. 2017), *prx01 prx44* and  
163 *prx01 prx73* (this study, not shown) as well as the triple null mutant, *prx01 prx44 prx73* showed  
164 similarly shorter root hair cells (**Figure 1B**) than what was previously reported for each of the  
165 individual *prx* mutants (Mangano et al. 2017). We also obtained two independent lines for each  
166 overexpressing PRXs fused to GFP and under the control of a strong *35SCaMV* promoter (PRX<sup>OE</sup>).  
167 Unlike the *prx01 prx44 prx73* triple mutant, the lines overexpressing PRX44 and PRX73 had  
168 significantly longer root hairs than the Wt Col-0 control (**Figure 2A–B**). The root hairs of the PRX01<sup>OE</sup>  
169 lines, however, were similar to those of Wt Col-0 (**Figure 2A–B**). We reasoned that the lack of  
170 enhanced root hair expansion in the PRX01<sup>OE</sup> lines could be due to reduced levels of overexpression  
171 compared to the PRX44<sup>OE</sup> and PRX73<sup>OE</sup> lines. However, based on the GFP signals in intact roots (**Figure**  
172 **2C**), we established that PRX01<sup>OE</sup> and PRX44<sup>OE</sup> are strongly expressed, whereas PRX73<sup>OE</sup> showed more  
173 moderate expression. Furthermore, the three PRX-GFP-fusion proteins were detected at the expected  
174 molecular weights in an immunoblot (**Figure 2D**), indicating that the tagged proteins are stable. The  
175 lack of root hair growth enhancement in PRX01<sup>OE</sup> line might be due to regulatory aspects on the  
176 protein activity rather than in the protein level. Together, these results highlight the partially  
177 redundant roles of PRX01, PRX44, and PRX73 as positive regulators of polar growth. This is in  
178 agreement with the negative effect of SHAM (salicylic hydroxylamino acid), a peroxidase activity  
179 inhibitor (Ikeda-Saito, Shelley et al. 1991; Davey and Fenna 1996), on root hair growth (Mangano et  
180 al. 2017). Here is important to highlight that a SHAM treatment produce a more drastic effect on root  
181 hair growth and on the inhibition on overall peroxidase activity in the roots (Mangano et al. 2017)  
182 than the triple mutant *prx01 prx44 prx73*, suggesting the implication of other unidentified PRXs.

183  
184 To confirm that our mutant and overexpressing lines had the expected changes in peroxidase activity,  
185 we measured *in vitro* total peroxidase activity using a guaiacol oxidation-based assay. The *prx01,44,73*  
186 roots showed reduced peroxidase activity (close to 50% reduction) (**Figure 1C**), whereas there was a  
187 40–50% increase in PRX73<sup>OE</sup> and an approximately 20% increase in PRX44<sup>OE</sup> (**Figure 2E**). Consistent  
188 with our root hair growth analysis (**Figure 2A**), PRX01<sup>OE</sup> showed normal peroxidase activity (**Figure**  
189 **2E**). The homeostasis and levels of ROS (mostly H<sub>2</sub>O<sub>2</sub>) that regulates polar growth of root hair cells  
190 (Mangano et al. 2017) is composed by apoplastic ROS (<sub>apo</sub>ROS) as well as cytoplasmic ROS pools  
191 (<sub>cyt</sub>ROS). Both pools of ROS, their homeostasis and levels are modulated by their transport from the  
192 apoplast to the cytoplasmic side by specific aquaporins (PIPs for plasma membrane intrinsic proteins)  
193 in plant cells (Dynowski et al., 2008; Hooijmaijers et al., 2012 Rodrigues et al. 2017). We hypothesized



194 that these three PRXs might change the levels of ROS, most probably H<sub>2</sub>O<sub>2</sub>, for their catalytic functions  
195 in the cell wall/apoplast. Therefore, we measured <sub>cyt</sub>ROS levels by oxidation of H<sub>2</sub>DCF-DA and <sub>apo</sub>ROS  
196 levels with the Amplex Ultra Red (AUR) probe in root hair tips. The *prx01,44,73* root hair tips showed  
197 lower levels of <sub>cyt</sub>ROS (**Figure 1D**) but increased <sub>apo</sub>ROS accumulation (**Figure 1E**) compared to Wt Col-  
198 0. The <sub>apo</sub>ROS levels were similar in PRX01<sup>OE</sup>, and slightly lower in PRX44<sup>OE</sup>, and PRX73<sup>OE</sup> lines when  
199 compared to Wt Col-0 (**Figure 2F**). These results suggest that PRX01, PRX44, and PRX73 function as  
200 apoplastic regulators of ROS-linked root hair cell elongation.

201  
202 Next, to further analyze the ultrastructure of the cell wall in growing root hairs, we analyzed Wt Col,  
203 PRX44<sup>OE</sup>, and *prx01,44,73* triple mutant roots treated or not with SHAM by transmission electron  
204 microscopy (**Figure 3A**). Much found thinner cell walls at the root hair tips of PRX44<sup>OE</sup> ( $0.74 \pm \text{SD } 0.24$   
205  $\mu\text{m}$  for PRX44<sup>OE</sup>) and *prx01,44,73* ( $0.61 \pm \text{SD } 0.14 \mu\text{m}$ ) when compared to Wt Col-0 plants ( $1.2 \pm \text{SD}$   
206  $0.3 \mu\text{m}$  for Wt) (**Figure 3B**). SHAM treatment caused a statistically significant increase in cell wall  
207 thickness in the PRX44<sup>OE</sup> and *prx01,44,73* root hairs (**Figure 3B**), but not in Wt Col-0. This result  
208 suggests the importance of peroxidase activity in cell wall structure and highlights that either  
209 depletion of PRX01,44,73 (triple mutant) or the overexpression of PRX44 results in an overall  
210 reduction in cell wall thickness in growing root hairs. This implies that the constitutive mis-regulation  
211 of PRX activity (either reduced/impaired function or overexpression) affects the capacity of root hairs  
212 to form normal cell walls and this clearly affects their cell expansion process.

213  
214 Then, we designed an EXT reporter to track EXT secretion and PRX-mediated insolubilization in the  
215 cell walls during root hair cell elongation. The secreted EXT reporter carries a Tomato tag (SS-TOM-  
216 Long-EXT) that is fluorescent under the acidic pH (Shen et al. 2014) that is typical of plant cell walls  
217 and apoplastic spaces (Stoddard & Rolland 2018). A secreted Tomato tag (ss-TOM) was used as a  
218 control (**Figure S2A**). The EXT domain includes only two Tyr, which are at the C-terminus and  
219 separated by 10 amino acids (Stratford et al., 2001). Expression of the EXT reporter was first tested in  
220 onion (*Allium cepa*) cells, and then the reporter was stably expressed in Arabidopsis root hairs (**Figure**  
221 **S2C-F**). In both cases, plasmolysis was used to retract the plasma membrane from the cell surface to  
222 show that the EXT reporter was localized in the cell walls. Using immunoblot analysis, we detected  
223 the full-length EXT-Tomato fusion protein, with possible O-glycan modifications, running as higher  
224 molecular weight bands than expected (**Figure S2B**). Importantly, the EXT reporter did not interfere  
225 with the polar growth of root hairs (**Figure S2D**), and, therefore, could be used to track changes in the  
226 *in situ* arrangement of cell wall EXTs. SS-TOM-Long-EXT is clearly secreted in the cell wall of growing  
227 root hairs (**Figure S2C**) but remains to be tested if these EXT reporter is mislocalized under an inhibited  
228 PRX environment (SHAM treated) or in *prx01,44,73* mutant background.

229  
230 We then assessed the level of crosslinking of EXT Tyr residues by measuring peptidyl-tyrosine (Tyr)  
231 and isodityrosine (IDT, dimerized Tyr) in EXT extracted from whole roots. We detected a significant



232 increase in peptidyl-Tyr in the *prx01,44,73* triple mutant relative to Wt Col-0, and slightly higher levels  
233 of IDT in EXTs extracted from the PRX73<sup>OE</sup> line (**Table 1**). By contrast, we identified strong  
234 downregulation of Tyr- and IDT-levels in the EXT under-*O*-glycosylation mutants *p4h5 sergt1-1*, and  
235 *sergt1-1 rra3* (**Table 1**). In these two double mutants, root hair growth is drastically inhibited  
236 (Velasquez et al. 2015a). PROLYL 4-HYDROXYLASE (P4H5), PEPTIDYL-SER GALACTOSYLTRANSFERASE  
237 (SGT1/SERGT1), and REDUCE RESIDUAL ARABINOSE 3 (RRA3) are key enzymes that modify EXT  
238 hydroxylation (P4H5) and EXT *O*-glycosylation (SERGT1 and RRA3) (Marzol et al. 2018). Specifically, it  
239 was shown that P4H5 is a 2-oxoglutarate (2OG) dioxygenase that catalyze the formation of trans-4-  
240 hydroxyproline (Hyp/O) from peptidyl-proline preferentially in an EXT context allowing these proteins  
241 to be *O*-glycosylated (Velasquez et al. 2011; Velasquez et al. 2015b). In the case of RRA3, together  
242 with RRA1–RRA2 homologous proteins (Egelund et al., 2007; Velasquez et al., 2011), they are thought  
243 to transfer the second arabinose to the sort glycan (composed by 4–5 units of L-arabinofuranose)  
244 attached to the Hyp in the EXT peptides. SERGT1 add the single galactose units to the serine in the  
245 repetitive motif of Ser-(Pro)<sub>3–5</sub> present in EXT and EXT-related proteins (Saito et al. 2014). These  
246 results are consistent with the notion that *O*-glycans strongly affect EXT Tyr crosslinking, as was  
247 previously suggested based on the drastically reduced root hair growth of the under-glycosylation  
248 mutants and *in vitro* crosslinking rates (Velasquez et al 2015a,b; Chen et al. 2015). We hypothesize  
249 that absent or low *O*-glycosylation of EXTs or an increase in PRX levels may trigger a reduction in the  
250 amount of peptidyl-Tyr and IDT levels in EXTs, with a putative concomitant increase in the amounts  
251 of higher-order Tyr crosslinks (trimers as Pulcherosine and tetramers as Di-IDT), thus inhibiting root  
252 hair growth. For technical reasons we could not measure the Pulcherosine and Di-IDT levels described  
253 before in EXTs (Brady et al., 1996; 1998; Held et al. 2004) to test this hypothesis. Further research is  
254 needed to decipher the *in vivo* regulation of Tyr crosslinking of EXTs by these three PRXs in plant cells.  
255

256 A major limitation in our understanding of how EXTs function in plant cell walls is the lack of a realistic  
257 full-length EXT protein model. We used coarse-grained molecular dynamics to build a larger model of  
258 a triple-helix EXT sequence, that includes 10 conserved repeats (SPPPPYVYSSPPPPYSPSPKVYYK, 250  
259 aminoacids in each polypeptide chain) (**Figure S3A–B**). Parameters for the *O*-glycosylated form of EXT  
260 were developed in this work (**Figure S4**). The EXT molecules were modeled in two different states: as  
261 a non-glycosylated trimeric helical conformation similar to animal collagen and in the *O*-glycosylated  
262 state, with 4 arabinose monosaccharides in each hydroxyproline. Those two states were simulated  
263 restraining both ends of the polypeptide chains, to model a fully extended helix (consistent with an  
264 “indefinitely long-EXT”), and without that restriction, to evaluate the conformation that an isolated  
265 10-repeat triple helix would adopt. The results indicate the importance of the triple-helix  
266 conformation in the overall stability of the protein and especially in the conservation of its fibril-like  
267 structure, in agreement with shorter-repeats single helix simulations performed previously  
268 (Velasquez et al. 2015a; Marzol et al. 2018). The total volume of the extended systems triple helix was  
269 measured in both glycosylation states (**Table S1**), differentiating EXT-protein-only and EXT-

270 protein+glycan volumes for the fully *O*-glycosylated EXT state. We observed that the EXT-protein-only  
271 volume was significantly augmented by the presence of the oligosaccharide moieties, indicating that  
272 *O*-glycans increase the distance between peptide chains in the EXT triple helix. We report the average  
273 diameters for those systems (**Table S1**), which are consistent with the diameters previously reported  
274 based on Atomic Force Microscopy (AFM) (images (Cannon et al. 2008). Additionally, *O*-glycosylation  
275 contributes to an increase in the average distance between the side chains of tyrosine residues,  
276 decreasing the proportion of tyrosine side chains that are close enough to lead to crosslinked EXT  
277 chains (**Figure S3C**). Current experimental and modeling lines of evidence are in agreement with the  
278 proposed role of proline-hydroxylation and carbohydrate moieties in keeping the EXT molecule in an  
279 extended helical polyproline-II conformation state (Stafstrom & Staehelin 1986; Owen et al., 2010;  
280 Ishiwata et al., 2014). This extended conformation might allow EXTs to interact properly with each  
281 other and with other components in the apoplast, including PRXs and pectins, to form a proper cell  
282 wall network (Nuñez et al., 2009; Valentin et al., 2010).

283  
284 To test if these three PRXs (PRX01, PRX44, and PRX73) might be able to interact with single-chain  
285 EXTs, we performed homology modeling with GvEP1, an EXT-PRX that is able to crosslink EXTs *in vitro*  
286 (Jackson et al., 2001; Pereira et al. 2011). In addition, we included PRX64, as a PRX described for lignin  
287 polymerization in the root endodermis (Lee et al. 2013) and PRX36, which is able to bind  
288 homogalacturonan pectin in the seed coat (Francoz et al. 2019) as controls. By *docking* analysis, we  
289 obtained interaction energies (Kcal/mol) for all of them. We analyzed docking with four different short  
290 EXT peptides: a non-hydroxylated peptide, a hydroxylated peptide, an arabinosylated peptide and an  
291 arabino-galactosylated peptide. As mentioned earlier, it was previously shown that mutants carrying  
292 under-*O*-glycosylated EXTs have severe defects in root hair growth (Velasquez et al. 2011; Velasquez  
293 et al. 2015a). Our docking results for the different PRXs show consistent interaction energy differences  
294 that depend on the EXT glycosylation state, being higher for non-*O*-glycosylated species. In addition,  
295 *O*-glycosylated EXT variants docked in a rather dispersed way while non-*O*-glycosylated variants  
296 preferentially docked in a grooved area (**Figure 4A–C**). Furthermore, **Figure 4A** shows how a non-*O*-  
297 glycosylated peptide binds through a groove, leaving one Tyr docked in a cavity and very close to the  
298 heme iron (5Å), with a second Tyr a few Angstroms away. The arrangement and distances between  
299 the tyrosines suggest that this could be an active site where Tyr crosslinking takes place. Although it  
300 is not possible to compare the interaction energies obtained with the different EXT species among  
301 docking runs, a general trend can be observed in **Figure 4C**. In general, we observed higher interaction  
302 energies (more negative values) for hydroxylated EXT species, followed by non-hydroxylated EXTs,  
303 and then by *O*-glycosylated EXT variants. When we compared interaction energies among different  
304 PRXs interacting with EXT substrates with the same degree of *O*-glycosylation, we observed that  
305 PRX73 displayed the highest interaction activity with the non-hydroxylated EXT species, followed by  
306 PRX01 and then PRX44. For the hydroxylated EXT variant, the order was PRX44>PRX73>PRX01. PRX44  
307 displayed the highest interaction energy with the *O*-glycosylated species. All together, these results

308 are consistent with the constitutive root hair growth effect observed for PRX44<sup>OE</sup> and PRX73<sup>OE</sup> and  
309 with non-glycosylated EXT being the substrate of peroxidation. Overall, this possibly indicates that  
310 PRX44 and PRX73 might interact with EXT substrates and possibly catalyze Tyr-crosslinking in open  
311 regions of the EXT backbones with little or no *O*-glycosylation. This is in agreement with previous  
312 studies that suggested that high levels of *O*-glycosylation in certain EXT segments physically restrict  
313 EXT lateral alignments, possibly by acting as a branching point (Cannon et al.2008; Velasquez et al.,  
314 2015a; Marzol et al. 2018).

315  
316 To examine the evolution of PRX01, PRX44, and PRX73, we performed comprehensive phylogenetic  
317 analyses of Class-III peroxidases across diverse land plant lineages. Under low selective pressure to  
318 maintain substrate specificity, EXT-PRX activities might have evolved multiple times in parallel during  
319 land plant evolution through gene duplication followed by neofunctionalization or  
320 subfunctionalization. PRX01, PRX44, and PRX73 belong to three independent orthologous groups  
321 (**Figure S5**) and orthologs for each *A. thaliana* PRX have been detected in available Brassicaceae  
322 genomes and in various Angiosperm and Gymnosperm families, but not from Lycophytes and from  
323 non-vascular land plants. Thus, these three PRX sequences were the result of ancestral duplications  
324 before the divergence between Gymnosperms and Angiosperms but after the emergence of the  
325 Tracheophytes (**Figure S5**). Orthologs of the three PRX genes have only been detected in true root  
326 containing organisms and these three PRXs are expressed in roots and root hairs, as are most of their  
327 orthologous sequences (where expression data are available) (**Figure S6**). This strongly supports the  
328 hypothesis that the three independent orthogroups have conserved functions in roots. With the  
329 exception of PRX73, which belongs to a cluster containing the putative EXT-PRX from tomato  
330 (*Solanum lycopersicum*; LePRX38), the other two PRX sequences did not cluster with sequences  
331 already described as putative EXT-PRXs, such as PRX09 and PRX40 (Jacobowitz et al. 2019). Indeed,  
332 the other known EXT-PRXs (identified mostly based on *in vitro* evidence) are not clustered together,  
333 but are widely distributed in the tree (**Figure S5**). This analysis suggests that plant EXT-PRXs might  
334 have evolved several times in parallel during Tracheophyte evolution.

335  
336 Based on the results shown in this work, we propose a working model in which PRX01, PRX44, and  
337 PRX73 (and possibly other PRXs) control root hair growth by channelling H<sub>2</sub>O<sub>2</sub> consumption and  
338 affecting the cell wall hardening process. In this polar growing cells, it is known that H<sub>2</sub>O<sub>2</sub> is primary  
339 derived from by the respiratory burst oxidase homolog C (RBOHC), and to a lower extent from RBOHH  
340 and RBOHJ activities that produce superoxide ions (Monshausen et al. 2007; Tajeda et al. 2008;  
341 Mangano et al. 2017) that are further converted chemically or enzymatically to H<sub>2</sub>O<sub>2</sub>. Then, part of  
342 H<sub>2</sub>O<sub>2</sub> might be transported from the apoplast to the cytoplasm side by specific PIPs as it was shown  
343 to occur in several plant cell types (e.g. in stomata and epidermal cells) in response to diverse stimuli  
344 (Dynowski et al., 2008; Hooijmaijers et al., 2012; Rodrigues et al. 2017). When apoplastic PRX protein  
345 levels are low, which is linked to reduced peroxidase activity as in the triple mutant *prx01,44,73*, high

346 levels of H<sub>2</sub>O<sub>2</sub> accumulate in the apoplast, triggering through the oxidative cycle (OC) a cell wall  
347 loosening effect that affects growth homeostasis and inhibits expansion by decreasing root hair  
348 growth and cell wall thickness (**Figure S7**). Concomitantly, deficient PRX activity in the apoplast also  
349 triggers lower H<sub>2</sub>O<sub>2</sub> levels in the cytoplasm of growing root hairs. This is in agreement with the fact  
350 that exogenously supplied H<sub>2</sub>O<sub>2</sub> inhibited root hair polar expansion, whereas treatment with ROS  
351 scavengers (e.g., ascorbic acid) caused root hair bursting (Orman-ligeza et al. 2016), reinforcing the  
352 notion that <sub>apo</sub>ROS modulates cell growth by impacting cell-wall properties (Mangano et al. 2017). Our  
353 results suggest that either low or high levels of apoplastic Class-III PRXs in the root hair cell walls might  
354 affect the homeostasis of ROS and cell wall thickness with a clear effect on cell expansion. Still several  
355 aspects of this model proposed here remains to be tested.

356

### 357 **Conclusions**

358 Currently, several of the 73 apoplastic Class-III PRXs in *Arabidopsis thaliana* have no assigned  
359 biological function. In this work, we have characterized three related EXT-PRXs, PRX01, PRX44, and  
360 PRX73 that function in ROS homeostasis and potentially in EXT assembly during root hair growth.  
361 These PRXs might control Tyr crosslinking in EXTs and related glycoproteins and modify its secretion  
362 and assembly in the nascent tip cell walls. Using modeling and docking approaches, we were able to  
363 measure the interactions of these PRXs with single chain EXT substrates. All these lines of evidence  
364 indicate that PRX01, PRX44, and PRX73 are important enzymes that could be involved in EXT assembly  
365 during root hair growth. From an evolutionary perspective, all the putative EXT-PRXs (previously  
366 identified based on *in vitro* evidence or immunolabeling) do not cluster together in the phylogenetic  
367 tree of Class-III PRXs, suggesting that plant-related EXT-PRXs might have evolved several times in  
368 parallel during Tracheophyte evolution. Interestingly, as a convergent evolutionary extracellular  
369 assembly, hydroxyproline-rich collagen Class-IV, similar to the green EXT lineage and related  
370 glycoproteins, is also crosslinked by the activity of a specific class of animal heme peroxidases (named  
371 peroxidasin or PXDN) to form insoluble extracellular networks (Vanacore et al. 2009; Bhave et al.  
372 2012). While the biophysical properties of collagen IV allow the correct development and function of  
373 multicellular tissues in all animal phyla (Brown et al. 2017), EXT assemblies also have key functions in  
374 several plant cell expansion and morphogenesis processes (Baumberger 2001, 2003; Hall and Cannon  
375 et al. 2002; Cannon *et al.*, 2008; Ringli 2010; Lamport et al., 2011; Velasquez et al. 2015a,b; Fabrice et  
376 al. 2018; Sede et al. 2018; Marzol et al. 2018). This might imply that crosslinked extracellular matrices  
377 based on hydroxyproline-rich polymers (e.g., collagens and EXTs) have evolved more than once during  
378 eukaryotic evolution, providing mechanical support to single and multiple cellular tissues. Further  
379 analyses are required to establish how these described EXT-PRXs catalyze Tyr crosslinks on EXTs at  
380 the molecular level and how this assembly process is regulated during polar cell expansion.

## 381 **Experimental Procedures**

382  
383 **Plant and growth conditions.** *Arabidopsis thaliana* Columbia-0 (Col-0) was used as the wild Class (Wt)  
384 genotype in all experiments. All mutants and transgenic lines tested are in this genetic background.  
385 Seedlings were germinated on agar plates in a Percival incubator at 22°C in a growth room with 16h  
386 light/8h dark cycles for 10 days at 140  $\mu\text{mol m}^{-2}\text{s}^{-1}$  light intensity. Plants were transferred to soil for  
387 growth under the same conditions. For identification of T-DNA knockout lines, genomic DNA was  
388 extracted from rosette leaves. Confirmation by PCR of a single and multiple T-DNA insertions in the  
389 target PRX genes were performed using an insertion-specific LBb1.3 primers in addition to one gene-  
390 specific primer. To ensure gene disruptions, PCR was also run using two gene-specific primers,  
391 expecting bands corresponding to fragments larger than in WT. We isolated homozygous lines for  
392 PRX01 (AT1G05240, *prx01-2*, Salk\_103597), PRX44 (AT4G26010, *prx44-2*, Salk\_057222) and PRX73  
393 (AT5G67400, *prx73-3*, Salk\_009296). SERGT1 (*sergt1-1* SALK\_054682), *rra3* (GABI\_233B05)  
394 (Velasquez et al., 2011) and *p4h5* T-DNA mutant (Velasquez et al., 2011) were isolated and described  
395 previously. Double and triple mutants were generated by manual crosses of the corresponding single  
396 mutants (Velasquez et al., 2015a). All the mutant lines used in this study are described in **Table S2**.

397  
398 **PRX::GFP and 35S::PRX-GFP lines.** Vectors based on the Gateway cloning technology (Invitrogen)  
399 were used for all manipulations. Constitutive expression of PRXs-GFP tagged lines were achieved in  
400 plant destination vector pMDC83. cDNA PRXs sequences were PCR-amplified with AttB recombination  
401 sites. PCR products were then recombined first in pDONOR207 and transferred into pGWB83. To  
402 generate transcriptional reporter, the PRXs promoter regions (2Kb) was amplified and recombined  
403 first in pDONOR207 and transferred into pMDC111. All the transgenic lines used in this study are  
404 described in **Table S2**.

405  
406 **SS-TOM and SS-TOM-Long-EXT constructs.** The binary vector pART27, encoding tdTomato secreted  
407 with the secretory signal sequence from tomato polygalacturonase and expressed by the constitutive  
408 CaMV 35S promoter (pART-SS-TOM), was the kind gift of Dr. Jocelyn Rose, Cornell University. The  
409 entire reporter protein construct was excised from pART-SS-TOM by digesting with *NotI*. The resulting  
410 fragments were gel-purified with the QIAquick Gel Extraction Kit and ligated using T4 DNA Ligase (New  
411 England Biolabs) into dephosphorylated pBlueScript KS+ that had also been digested with *NotI* and  
412 gel-purified to make pBS-SS-TOM. The plasmid was confirmed by sequencing with primers 35S-FP (5'-  
413 CCTTCGCAAGACCCTCCTC-3') and OCS-RP (5'-CGTGCACAACAGAATTGAAAGC-3'). The sequence of the  
414 EXT domain from *SIPEX1* (NCBI accession AF159296) was synthesized and cloned by GenScript into  
415 pUC57 (pUC57-EXT). The plasmid pBS-SS-TOM-Long-EXT was made by digesting pUC57-EXT and pBS-  
416 SS-TOM with *NdeI* and *SgrAI*, followed by gel purification of the 2243 bp band from pUC57-EXT and  
417 the 5545 bp band from pBS-SS-TOM, and ligation of the two gel-purified fragments. The pBS-SS-TOM-  
418 Long-EXT plasmid was confirmed by sequencing with 35S-FP, OCS-RP, and tdt-seq-FP (5'-



419 CCCGTTCAATTGCCTGGT-3'). Both pBS plasmids were also confirmed by digestion. The binary vector  
420 pART-SS-TOM-Long-EXT was made by gel purifying the *NotI* insert fragment from the pBS-SS-TOM-  
421 Long EXT plasmid and ligating it with pART-SS-TOM backbone that had been digested with *NotI*, gel  
422 purified, and dephosphorylated. This plasmid was confirmed by sequencing. The construct SS-TOM  
423 and SS-TOM-Long-EXT were transformed into *Arabidopsis* plants. The secretory sequence (SS) from  
424 tomato polygalacturonase is MVIQRNSILLIIIFASSISTCRSGT (2.8kDa) and the EXT-Long domain  
425 sequence with six alanine cluster is  
426 BAAAAAAAACTLPSLKNFTFSKNIFESMDETCRPSSESKQVKIDGNENCLGGRSEQRTEKECFPVVSKPVDCSKGHCG  
427 VSREGQSPKDPKTVTTPPKPSTPTTPKPNPSPPPPKTLPPPKTSPPPPVHSPPPPVASPPPPVHSPPPPVASPPPP  
428 VHSPPPPVASPPPPVHSPPPPVASPPPPVHSPPPPVHSPPPPVASPPPPVHSPPPPVHSPPPPVHSPPPVHSPPP  
429 PVHSPPPPVASPPPPVHSPPPPVHSPPPPVHSPPPPVASPPPPVHSPPPPVASPPPPVHSPPPPVASPPPPVHSP  
430 PPPVASPPPPVHSPPPPVHSPPPPVHSPPPPVASPPPALVFSPPPPVHSPPPAPVMSPPPPTFEDALPPTLGSLYAS  
431 PPPPIFQGY\*395-(39.9kDa). The predicted molecular size for SS-TOM protein is 54.2 kDa and for SS-  
432 TOM-EXT-Long Mw is 97.4 kDa. All the transgenic lines used in this study are described in **Table S2**.

433  
434 **Root hair phenotype.** For quantitative analysis of root hair phenotypes in *prx01,44,73* mutant,  
435 35S:PRX-GFP lines and Wt Col-0, 200 fully elongated root hairs were measured (n roots= 20-30) from  
436 seedlings grown on vertical plates for 10 days. Values are reported as the mean  $\pm$ SD using the Image  
437 J software. Measurements were made after 7 days. Images were captured with an Olympus SZX7  
438 Zoom microscope equipped with a Q-Colors digital camera.

439  
440 **Confocal imaging.** Root hairs were ratio imaged with the Zeiss LSM 710 laser scanning confocal  
441 microscope (Carl Zeiss) using a 40X oil-immersion, 1.2 numerical aperture. EGFP (473–505nm)  
442 emission was collected using a 458-nm primary dichroic mirror and the meta-detector of the  
443 microscope. Bright-field images were acquired simultaneously using the transmission detector of the  
444 microscope. Fluorescence intensity was measured in 7  $\mu$ m ROI (Region Of Interest) at the root hair  
445 apex.

446  
447 **Peroxidase activity.** Soluble proteins were extracted from roots grown on agar plates in a Percival  
448 incubator at 22°C in a growth room for 10 days at 140  $\mu$ mol m<sup>-2</sup>s<sup>-1</sup> light intensity by grinding in 20mM  
449 HEPES, pH 7.0, containing 1 mM EGTA, 10mM ascorbic acid, and PVP PolyclarAT (100mg g<sup>-1</sup> fresh  
450 material; Sigma, Buchs, Switzerland). The extract was centrifuged twice for 10 min at 10,000 g. Each  
451 extract was assayed for protein levels with the Bio-Rad assay (Bio-Rad). PRX activity was measured at  
452 25°C by following the oxidation of 8 mM guaiacol (Fluka) at 470 nm in the presence of 2 mM H<sub>2</sub>O<sub>2</sub>  
453 (Carlo Erba) in a phosphate buffer (200 mM, pH6.0). Values are the mean of three replicates  $\pm$  SD.

454  
455 **Cytoplasmic ROS (cytROS) measurements.** 2',7'-dichlorodihydrofluorescein diacetate (H<sub>2</sub>DCF-DA) is  
456 as a cell-permeable fluorogenic probe to quantify reactive oxygen species (ROS). H<sub>2</sub>DCFDA diffuses

457 into cells and is deacetylated by cellular esterases to form 2',7'-dichlorodihydrofluorescein (H<sub>2</sub>DCF).  
458 In the presence of ROS, predominantly H<sub>2</sub>O<sub>2</sub>, H<sub>2</sub>DCF is rapidly oxidized to 2',7'-dichlorofluorescein  
459 (DCF), which is highly fluorescent, with excitation and emission wavelengths of 498 and 522 nm,  
460 respectively. To measure cytoplasmic ROS in root hairs cells, growth of Arabidopsis seeds on a plate  
461 was done with 1% sterile agar for 8 d in a chamber at 22°C with continuous light. These seedlings were  
462 incubated in darkness on a slide for 10 min with 50 μM H<sub>2</sub>DCFDA at room temperature. Samples were  
463 observed with Zeiss Imager A2 Epifluorescence. A 10× objective was used, 0.30 N.A., and exposure  
464 time 80-500ms. Images were analyzed using ImageJ 1.50b software. To measure ROS mean, a circular  
465 region of interest (ROI) (r=2.5) was chosen in the tip zone of the root hair. All root hairs of six seedlings  
466 per genotype were analyzed. The reported values are the mean ± standard deviation (mean ± SD).

467  
468 **Apoplasmic ROS (apoROS) measurements.** To measure apoplasmic ROS in root hair cells, roots of 7-day-  
469 old seedlings were incubated with 50 μM Amplex™ UltraRed Reagent (AUR, Molecular Probes) for 20  
470 min in dark conditions and rinsed with liquid MS. Root hairs were imaged with a Zeiss LSM5 Pascal  
471 laser scanning confocal microscope. The fluorescence emission of oxidized AUR in the apoplast of root  
472 hair cells was observed between 585 and 610 nm using 543 nm argon laser excitation, 40X objective,  
473 N/A=1.2. The intensity of fluorescence was quantified on digital images using ImageJ software.  
474 Quantification of the AUR probing fluorescence signal was restricted to apoplasmic spaces at the root  
475 hair tip (as shown in **Figure 1**). The measurements were performed in three independent experiments  
476 (n = 6) with the same microscopic settings.

477  
478 **Phylogenetic analysis.** 73 class-III PRX protein sequences from *A. thaliana*, two putative lignin class-  
479 III PRXs from *Zinnia elegans* and 4 putative Extensin class-III PRXs from *Lupinus album*, *Lycopersicon*  
480 *esculentum*, *Phaseolus vulgaris* and *Vitis vinifera*, have been aligned with ClustalW and the tree  
481 constructed using the Neighbor-Joining method (Saitou and Nei, 1987). The analyses were conducted  
482 in MEGA7 (Kumar, 2016). All protein sequences are available using their ID number  
483 (<http://peroxibase.toulouse.inra.fr>) (Savelli et al., 2019).

484  
485 **Co-expression analysis network.** Co-expression networks for *RSL4* root hair genes were identified  
486 from PlaNet (<http://aranet.mpimp-golm.mpg.de>) and trimmed to facilitate readability (Mutwill et al.  
487 2011). Each co-expression of interest was confirmed independently using the expression angler tool  
488 from Botany Array Resource BAR ([http://bar.utoronto.ca/ntools/cgi-](http://bar.utoronto.ca/ntools/cgi-bin/ntools_expression_angler.cgi)  
489 [bin/ntools\\_expression\\_angler.cgi](http://bar.utoronto.ca/ntools/cgi-bin/ntools_expression_angler.cgi)) and ATTED-II (<http://atted.jp>). Only those genes that are  
490 connected with genes of interest are included.

491  
492 **Tyr-crosslinking analysis.** Alcohol-insoluble residues of root tissues obtained from *PRX01,44,73*  
493 mutants, Col-0 and 35Sp::PRX44-GFP lines were hydrolyzed in 6 N HCl (aqueous) with 10 mM phenol  
494 (2 mg ml<sup>-1</sup>; 110 °C; 20 h). Hydrolysates were dried under a steady stream of nitrogen (gas) and then



495 re-dissolved at 10 mg ml<sup>-1</sup> in water. The hydrolysates were fractionated by gel permeation  
496 chromatography on a polyhydroxyethyl A column (inner diameter, 9.4 x 200 mm, 10 nm pore size,  
497 Poly LC Inc., Columbia, MD) equilibrated in 50 mM formic acid and eluted isocratically at a flow rate  
498 of 0.8 ml min<sup>-1</sup>. UV absorbance was monitored at 280 nm. The amounts of Tyr and IDT in the  
499 hydrolysates were then determined by comparison with peak areas of authentic Tyr and IDT  
500 standards. Response factors were determined from three level calibrations with the Tyr and IDT  
501 standards.

502  
503 **Immuno-blot Analysis.** Plant material (100 mg of root from 15 days old seedlings grown as indicated  
504 before) was collected in a microfuge tube and ground in liquid nitrogen with 400 mL of protein  
505 extraction buffer (125 mM Tris-Cl, pH. 4.4, 2% [w/v] SDS, 10% [v/v] glycerol, 6M UREA, 1% [v/v] b-  
506 mercaptoethanol, 1mM PMSF). Samples were immediately transferred to ice. After 4° centrifugations  
507 at 13000 rpm for 20 min, supernatant was move to a new 1.5 ml tube and equal volumes of Laemlli  
508 buffer (125 mM Tris-Cl, pH. 7.4, 4% [w/v] SDS, 40% [v/v] glycerol, 10% [v/v] β-mercaptoethanol,  
509 0.002% [w/v] bromphenol blue) were added. The samples (0.5–1.0 mg/mL of protein) were boiled for  
510 5 min and 30 mL were loaded on 10% SDS-PAGE. The proteins were separated by electrophoresis and  
511 transferred to nitrocellulose membranes. Anti-GFP mouse IgG (clones 7.1 and 13.1; Roche Applied  
512 Science) was used at a dilution of 1:2,000 and it was visualized by incubation with goat anti-mouse  
513 IgG secondary antibodies conjugated to horseradish peroxidase (1:2,000) followed by a  
514 chemiluminescence reaction (Clarity Western ECL Substrate; Bio-rad). For the SS-TOM lines analysis,  
515 proteins were extracted in 2x SDS buffer (4% SDS, 125mM Tris pH 6.8, 20% glicerol, 0.01%  
516 bromophenol blue, 50 mM dithiothreitol [DTT]), using 10 µl of buffer per mg of plant tissues of Wt  
517 Col-0, transgenic lines 35S:SS-TOM and 35S:SS-TOM-Long-EXT. Two transgenic lines were analyzed.  
518 10 µl of supernatant of each protein extract were run into a 12% polyacrylamide gel during one hour  
519 at 200 V, and then transferred to a PVDF membrane. PVDF was blocked with 5% milk in TBST (Tris-HCl  
520 10 mM, pH 7,4, NaCl 150 mM, Tween-20 al 0,05%) for 1 hour at 4°C and then washed four times  
521 during 15 min in TBST. An anti-RFP (A00682, GenScript) was used as primary antibody overnight at  
522 4°C. Four washes of 15 min each in TBST at room temperature and then it was incubated two hours  
523 with a secondary antibody anti-rabbit (goat) conjugated with alkaline phosphatase (A3687, Sigma), in  
524 a 1:2,500 dilution with TBST. Four washes of 15 min each in TBST at room temperature. Finally, 10 ml  
525 of alkaline phosphatase (100mM Tris-HCl pH 9.5, 100 mM NaCl, 3 mM MgCl<sub>2</sub>) containing 80 µl NBT  
526 (Sigma) (35mg/ml in 70% DMSO and 30 µl de BCIP (Sigma) (50 mg/ml in 100% de DMSO) were used.

527  
528 **Transmission electron microscopy of root hair cell walls.** Seeds were germinated on 0.2x MS, 1%  
529 sucrose, 0.8% agar. Seven days after germination, seedlings were transferred to new 0.2x MS, 1%  
530 sucrose, 0.8% agar plates with or without 100 µM SHAM. After 4 additional days, 1-mm root segments  
531 with root hairs were fix in 2% glutaraldehyde in 0.1M cacodylate buffer pH7.4. Samples were rinsed  
532 in cacodylate buffer and post-fixed in 2% OsO<sub>4</sub>. After dehydration in ethanol and acetone, samples

533 were infiltrated in Epon resin (Ted Pella, Redding, CA). Polymerization was performed at 60°C.  
534 Sections were stained with 2% uranyl acetate in 70% methanol followed by Reynold's lead citrate  
535 (2.6% lead nitrate and 3.5% sodium citrate [pH 12.0]) and observed in a Tecnai 12 electron  
536 microscope. Quantitative analysis of cell wall thickness was performed using FIJI.

537  
538 **Modeling and molecular docking between PRXs and EXTs.** Modeling and molecular docking: cDNA  
539 sequences of PRXs were retrieved from TAIR (PRX01: AT1G05240, PRX36: AT3G50990, PRX44:  
540 AT4G26010, PRX64: AT5G42180, PRX73: AT5G67400) and NCBI Nucleotide DB (PRX24Gv:Vitis vinifera  
541 peroxidase 24, GvEP1, LOC100254434). Homology modeling was performed for all PRXs using  
542 modeller 9.14 (Sali et al. 1993), using the crystal structures 1PA2, 3HDL, 1QO4 and 1HCH as templates,  
543 available at the protein data bank. 100 structures were generated for each protein and the best  
544 scoring one (according to DOPE score) was picked. The *receptor* for the docking runs was generated  
545 by the prepare\_receptor4 script from autodock suite, adding hydrogens and constructing bonds.  
546 Peptides based on the sequence PYYSPSPKVYYPPSSYVYPPPPS were used, replacing proline by  
547 hydroxyproline, and/or adding *O*-Hyp glycosylation with up to four arabinoses per hydroxyproline in  
548 the fully glycosylated peptide and a galactose on the serine, as it is usual in plant *O*-Hyp  
549 <https://www.ncbi.nlm.nih.gov/pmc/articles/PMC5045529/>. Ligand starting structure was generated  
550 as the most stable structure by molecular dynamics (Velasquez et al. 2015a). All ligand bonds were  
551 set to be able to rotate. Docking was performed in two steps, using Autodock vina (Trott et al. 2010).  
552 First, an exploratory search over the whole protein surface (exhaustiveness 4) was done, followed by  
553 a more exhaustive one (exhaustiveness 8), reducing the search space to a 75x75x75 box centered over  
554 the most frequent binding site found in the former run.

555  
556 **EXT conformational coarse-grained model.** The use of coarse-grained (CG) molecular dynamics (MD)  
557 allowed collection of long timescale trajectories. System reduction is significant when compared to all  
558 atom models, approximately reducing on order of magnitude in particle number. In addition, a longer  
559 integration time step can be used. Protein residues and coarse grained solvent parameters  
560 correspond to the SIRAH model (Darré et al. 2015), while ad hoc specific glycan parameters were  
561 developed. The CG force field parameters developed correspond to arabinofuranose and  
562 galactopyranose (**Figure S5**). Triple helix systems were simulated both, in the non-glycosylated and  
563 fully *O*-glycosylated states, where all the hydroxyprolines are bound to a tetrasaccharide of  
564 arabinofuranoses, and specific serine residues contain one galactopyranose molecule. They were  
565 immersed in WT4 GC solvent box that was constructed to be 2 nm apart from the extensin fiber, and  
566 periodic boundary conditions were employed. Coarse grained ions were also included to achieve  
567 electroneutrality and 0.15 M ionic strength. All simulations were performed using the GROMACS MD  
568 package at constant temperature and pressure, using the Berendsen thermostat (respectively) and  
569 Parrinello-Rahman barostat (Parrinello and Rahman 1981), and a 10 fs time step. The obtained  
570 trajectories were analysed using the Mdtraj python package (McGibbon et al, 2015) and visualized

571 with Visual Molecular Dynamics (VMD) 1.9.1 (Humphrey et al. 1996). Volume measurements were  
572 performed using a Convex Hull algorithm implemented in NumPy (Oliphant 2006), and average  
573 diameter calculations were derived from this quantity using simple geometric arguments.

574 **Acknowledgements**

575 We thank Andres Rossi from the microscopy facility of FIL for his assistance. We thank ABRC (Ohio  
576 State University) for providing T-DNA lines seed lines. J.M.E. is Principal Investigator of the National  
577 Research Council (CONICET) from Argentina. This work was supported by grants from ANPCyT  
578 (PICT2016-0132 and PICT2017-0066) and a grant from ICGEB CRP/ARG16-03 to J.M.E. In addition, this  
579 research is also funded by Instituto Milenio iBio–Iniciativa Científica Milenio, MINECON to J.M.E. and  
580 NSF MCB grant 1614965 to M.S.O.

581

582 **Author Contribution**

583 E.M and C.B performed most of the experiments and analysed the data. P.R. and C.D. analysed the  
584 peroxidase activity and performed phylogenetic analysis. J.W.M-E and M.H. analysed the Tyr-  
585 crosslinking on EXTs. A.A.A. and A.D.N performed the docking experiments and analysed this data.  
586 M.B. and L.C. perform the EXT modelling and analysed this data. M.F. and P.B generated the EXT  
587 reporter lines and performed the immune-blot analysis of SS-TOM and SS-TOM-Long-EXT lines.  
588 J.M.P., D.R.R.G., Y.d.C.R.G., S.M., and F.B.H. analysed the data. J.P., J.P-V., and M.S.O. performed the  
589 transmission electron microscopy analysis. J.M.E. designed research, analysed the data, supervised  
590 the project, and wrote the paper. All authors commented on the results and the manuscript. This  
591 manuscript has not been published and is not under consideration for publication elsewhere. All the  
592 authors have read the manuscript and have approved this submission.

593

594 **Competing financial interest**

595 The authors declare no competing financial interests. Correspondence and requests for materials  
596 should be addressed to J.M.E. (Email: [jestevez@leloir.org.ar](mailto:jestevez@leloir.org.ar) / [jose.estevez@unab.cl](mailto:jose.estevez@unab.cl)).

597 **REFERENCES**

- 598 Baumberger N, Ringli C, Keller B. (2001). The chimeric leucine rich repeat/extensin cell wall protein  
599 LRX1 is required for root hair morphogenesis in *Arabidopsis thaliana*. *Genes & Development* 15,  
600 1128–1139.
- 601 Baumberger N, Steiner M, Ryser U, Keller B, Ringli C. (2003). Synergistic interaction of the two  
602 paralogous Arabidopsis genes LRX1 and LRX2 in cell wall formation during root hair development.  
603 *Plant J.* 35, 71–81.
- 604 Berendsen, H. J. C., Postma, J.P.M., van Gunsteren, W.F., DiNola, A., and Haak, J.R. (1984) Molecular  
605 dynamics with coupling to an external bath. *J. Chem. Phys.* 81, 3684. doi: 10.1063/1.448118.
- 606 Berman HM, John Westbrook, Zukang Feng, Gary Gilliland, Talapady N Bhat, Helge Weissig, Ilya N  
607 Shindyalov, and Philip E Bourne. The protein data bank. *Nucleic Acids Research*, 28(1):235–242,  
608 2000.
- 609 Bernards, M.A., Fleming, W.D., Llewellyn, D.B., Priefer, R., Yang, X., Sabatino, A., and Plourde, G.L.  
610 (1999). Biochemical characterization of the suberization-associated anionic peroxidase of potato.  
611 *Plant Physiol.* 121: 135–146.
- 612 Bhave G, Cummings CF, Vanacore RM, Kumagai-Cresse C, Ero-Tolliver IA, Rafi M, Kang J-S, Pedchenko  
613 V, Fessler LI, Fessler JH, Hudson BG (2012) Peroxidase forms sulfilimine chemical bonds using  
614 hypohalous acids in tissue genesis. *Nat. Chem. Biol.* 8:784–790.
- 615 Brady, J.D., Sadler, I.H., and Fry, S.C. (1996). Di-isodityrosine, a novel tetrameric derivative of tyrosine  
616 in plant cell wall proteins: a new potential cross-link. *Biochem. J* 315: 323–327.
- 617 Brady, J.D., Sadler, I.H., and Fry, S.C. (1998). Pulcherosine, an oxidatively coupled trimer of tyrosine in  
618 plant cell walls: its role in cross-link formation. *Phytochemistry.* 47(3):349-353.
- 619 Brown K.L, C.F. Cummings, R.M. Vanacore and B.G. Hudson. (2017). Building collagen IV smart  
620 scaffolds on the outside of cells. *Protein Sci.* 26:2151-2161.
- 621 Brownleader, M.D., Ahmed, N., Trevan, M., Chaplin, M.F., and Dey, P.M. (1995). Purification and  
622 partial characterization of Tomato extensin peroxidase. *Plant Physiol.* 109: 1115–1123
- 623 Cannon, M.C., Terneus, K., Hall, Q., Tan, L., Wang, Y., Wegenhart, B.L., Chen, L., Lamport, D.T., Chen,  
624 Y., and Kieliszewski, M.J. (2008). Self-assembly of the plant cell wall requires an extensin scaffold.  
625 *Proc. Natl. Acad. Sci. USA.* 105: 2226–2231.
- 626 Chen, Y., Dong, W., Tan, L., Held, M. A., & Kieliszewski, M. J. (2015). Arabinosylation plays a crucial  
627 role in extensin cross-linking in vitro. *Biochemistry insights*, 8, BCI-S31353.
- 628 Cosio C. & Dunand C. (2009). Specific functions of individual class III peroxidases genes. *J. Exp. Bot.*  
629 62:391–408.
- 630 Cosio C., Ranocha Ph., Francoz E., Burlat V., Zheng Y., Perry S.E., Ripoll J.-J., Yanofsky M., Dunand C.  
631 (2017) The class III peroxidase PRX017 is a direct target of the MADS-box transcription factor 1  
632 AGL15 and participates in lignified tissue formation. *New Phytol.* 213: 250-263.
- 633 Darré, L., Machado, M.R., Brandner, A.F., González, H.C., Ferreira, S., and Pantano, S. (2015). SIRAH:  
634 A structurally unbiased coarse-grained force field for proteins with aqueous solvation and long-  
635 range electrostatics. *J. Chem. Theory Comput.* 11(2):723–739.
- 636 Davey, C. A. and R. E. Fenna (1996). 2.3 Å resolution X-ray crystal structure of the bisubstrate analogue  
637 inhibitor salicylhydroxamic acid bound to human myeloperoxidase: a model for a prereaction  
638 complex with hydrogen peroxide. *Biochemistry* 35(33): 10967-10973.

- 639 Dong, W., Kieliszewski, M., and Held, M.A. (2015). Identification of the pl 4.6 extensin peroxidase from  
640 *Lycopersicon esculentum* using proteomics and reverse-genomics. *Phytochem.* 112:151–159.
- 641 Dunand, C., Crevecoeur, M., and Penel, C. (2007). Distribution of superoxide and hydrogen peroxide  
642 in Arabidopsis root and their influence on root development: possible interaction with  
643 peroxidases. *New Phytol.* 174:332–341.
- 644 Dynowski M, Schaaf G, Loque D, Moran O, Ludewig U (2008) Plant plasma membrane water channels  
645 conduct the signalling molecule H<sub>2</sub>O<sub>2</sub>. *Biochem J* 414: 53–56.
- 646 Egelund, J., Obel, N., Ulvskov, P., Geshi, N., Pauly, M., Bacic, A., and Larsen Petersen, B. (2007).  
647 Molecular characterization of two Arabidopsis thaliana glycosyltransferase mutants, rra1 and  
648 rra2, which have a reduced residual arabinose content in a polymer tightly associated with the  
649 cellulosic wall residue. *Plant. Mol. Biol.* 64:439–451.
- 650 Fabrice T, Vogler H, Draeger C, Munglani G, Gupta S, Herger A, Knox P, Grossniklaus U, Ringli C. (2018).  
651 LRX Proteins play a crucial role in pollen grain and pollen tube cell wall development. *Plant*  
652 *Physiology* 176: 1981–1992.
- 653 Francoz et al. (2019) Pectin demethylesterification generates platforms that anchor peroxidases to  
654 remodel plant cell wall domains. *Developmental Cell* 48, 1-16.
- 655 Hall, Q., and Cannon, M.C. (2002). The cell wall hydroxyproline-rich glycoprotein RSH is essential for  
656 normal embryo development in Arabidopsis. *Plant Cell* 14: 1161–1172.
- 657 Held, M. A., Tan, L., Kamyab, A., Hare, M., Shpak, E., and Kieliszewski, M. J. (2004). Di-isodityrosine is  
658 the intermolecular cross-link of isodityrosine-rich extensin analogs cross-linked in vitro. *Journal of*  
659 *Biological Chemistry*, 279(53), 55474-55482.
- 660 Herrero, J., Fernández-Pérez, F., Yebra, T., Novo-Uzal, E., Pomar, F., Pedreño, M.Á., Cuello, J., Guéra,  
661 A., Esteban-Carrasco, A., and Zapata, J.M. (2013). Bioinformatic and functional characterization of  
662 the basic peroxidase 72 from Arabidopsis thaliana involved in lignin biosynthesis. *Planta* 237:  
663 1599–1612.
- 664 Hooijmaijers C, Rhee JY, Kwak KJ, Chung GC, Horie T, Katsuhara M, Kang H (2012) Hydrogen peroxide  
665 permeability of plasma membrane aquaporins of *Arabidopsis thaliana*. *J Plant Res* 125: 147–153.
- 666 Humphrey, W., Dalke, A., and Schulten, K. (1996). VMD: Visual molecular dynamics. *J. Molec. Graphics*  
667 14:33-38
- 668 Ikeda-Saito, M., D. A. Shelley, L. Lu, K. Booth, W. Caughey and S. Kimura (1991). Salicylhydroxamic acid  
669 inhibits myeloperoxidase activity. *Journal of Biological Chemistry* 266(6): 3611-3616
- 670 Ishiwata A, Kaeothip S, Takeda Y, Ito Y (2014) Synthesis of the highly glycosylated hydrophilic motif of  
671 extensins. *Angew Chem Int Ed Engl* 53: 9812–9816
- 672 Jackson, P.A., Galinha, C.I., Pereira, C.S., Fortunato, A., Soares, N.C., Amâncio, S.B., and Pinto Ricardo,  
673 C.P. (2001). Rapid deposition of extensin during the elicitation of grapevine callus cultures is  
674 specifically catalyzed by a 40-kilodalton peroxidase. *Plant Physiol.* 127: 1065–1076.
- 675 Jacobowitz, J.R, Doyle W.C., and Weng, J-K. (2019). PRX9 and PRX40 are extensin peroxidases essential  
676 for maintaining tapetum and microspore cell wall integrity during Arabidopsis anther  
677 development. *Plant Cell* 31: 848–86.
- 678 Kim D Pruitt, Tatiana Tatusova, and Donna R Maglott. Ncbi reference sequences (refseq): a curated  
679 non-redundant sequence database of genomes, transcripts and proteins. *Nucleic Acids Research*,  
680 35(suppl 1):D61–D65, 2006.
- 681 Kumar, S., Stecher G., Tamura K. (2016) MEGA7: molecular evolutionary genetic analysis version 7.0  
682 for bigger datasets. *Mol. Biol. Evol.* 33(7): 1870-1874.

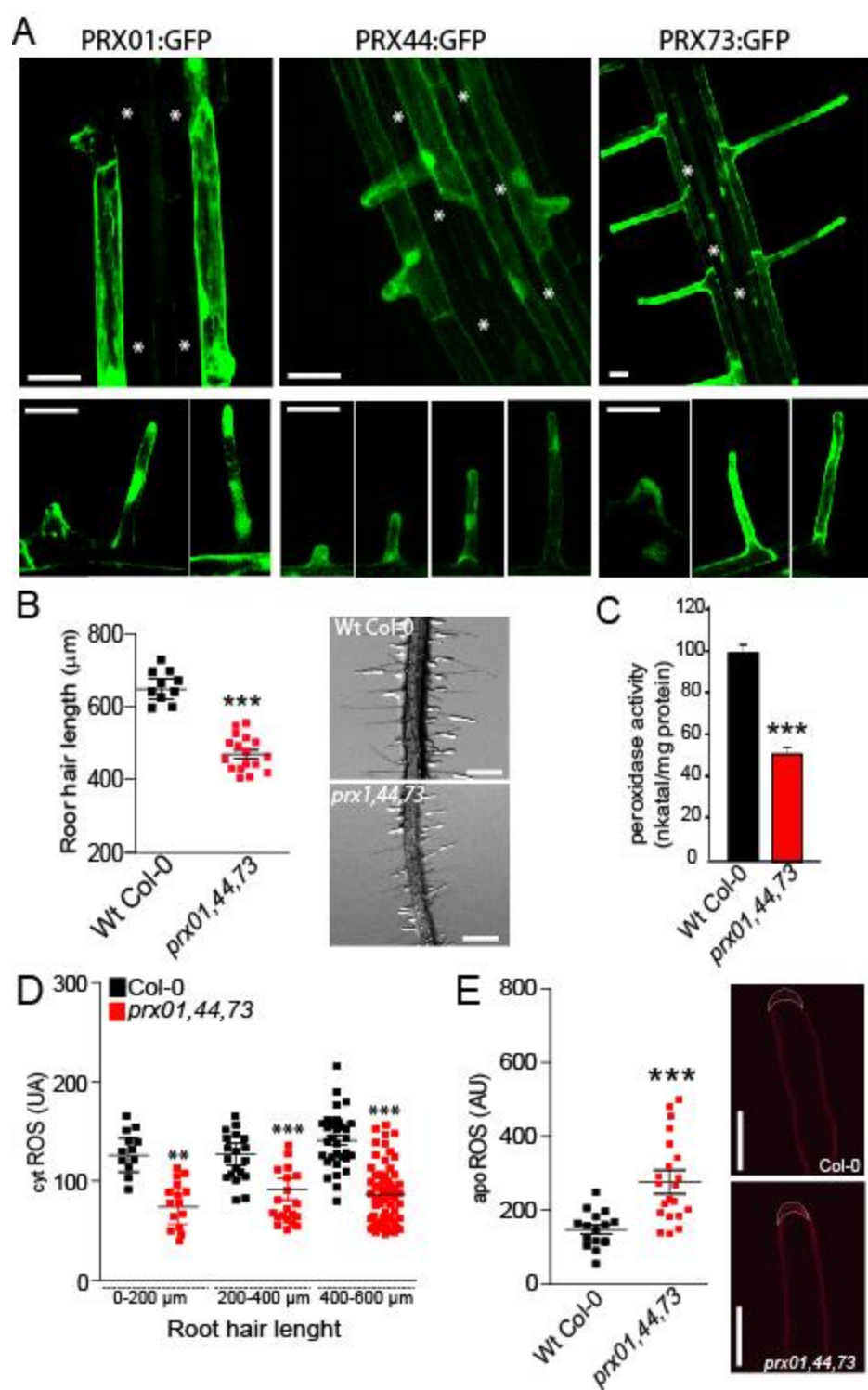


- 683 Kunieda, T., Shimada, T., Kondo, M., Nishimura, M., Nishitani, K., and Hara-Nishimura, I. (2013).  
684 Spatiotemporal secretion of PEROXIDASE36 is required for seed coat mucilage extrusion in  
685 Arabidopsis. *Plant Cell* 25: 1355–1367.
- 686 Lamport, D.T.A., Kieliszewski, M.J., Chen, Y., and Cannon, M.C. (2011). Role of the extensin  
687 superfamily in primary cell wall architecture. *Plant Physiol.* 156: 11–19.
- 688 Lee, Y., Rubio, M.C., Alassimone, J., and Geldner, N. (2013). A mechanism for localized lignin  
689 deposition in the endodermis. *Cell* 153: 402–412.
- 690 Mangano S. *et al.* (2017). The molecular link between auxin and ROS-controlled root hair growth.  
691 *Proc. Natl. Acad. Sci. U.S.A.* 114(20):5289-5294.
- 692 Marzol E, Borassi C, Bringas M, Sede A, Rodríguez Garcia DR, Capece L, Estevez JM. (2018). Filling the  
693 Gaps to Solve the Extensin Puzzle. *Mol Plant.* 11(5):645-658.
- 694 McGibbon R.T, Beauchamp K.A., Harrigan M.P., Klein C., Swails, J.M., Hernández C.X., Schwantes C.R.,  
695 Wang, L.P., Lane T.J., Pande V.S. (2015) MDTraj: A Modern Open Library for the Analysis of  
696 Molecular Dynamics Trajectories. *Biophysical Journal*, 109(8): 1528-1532.
- 697 Møller, S.R., et al. (2017). Identification and evolution of a plant cell wall specific glycoprotein glycosyl  
698 transferase, ExAD. *Sci. Rep.* 7: 45341.
- 699 Monshausen GB, Bibikova TN, Messerli MA, Shi C, Gilroy S (2007) Oscillations in extracellular pH and  
700 reactive oxygen species modulate tip growth of Arabidopsis root hairs. *Proc Natl Acad Sci USA*  
701 104:20996–21001.
- 702 Mutwil, M., Klie, S., Tohge, T., Giorgi, F.M., Wilkins, O., Campbell, M.M., Fernie, A.R., Usadel, B.,  
703 Nikoloski, Z. and Persson, S. (2011). PlaNet: combined sequence and expression comparisons  
704 across plant networks derived from seven species. *Plant Cell*, 23, 895– 910.
- 705 Oliphant, TE. USA: Trelgol Publishing, (2006). A guide to NumPy. 376 pp.
- 706 Orman-Ligeza B, et al. (2016) RBOH-mediated ROS production facilitates lateral root emergence in  
707 Arabidopsis. *Development* 143:3328–3339
- 708 Owens NW, Stetefeld J, Lattová E, Schweizer F (2010) Contiguous O-galactosylation of 4(R)-hydroxy-l-  
709 proline residues forms very stable polyproline II helices. *J Am Chem Soc* 132: 5036–5042
- 710 Parrinello, M. and Rahman, A. (1981). Polymorphic transitions in single crystals: A new molecular  
711 dynamics method. *J. of Applied Physics* 52:7182. doi.org/10.1063/1.328693
- 712 Passardi, F., Penel, C., and Dunand, C. (2004). Performing the paradoxical: how plant peroxidases  
713 modify the cell wall. *Trends Plant Sci.* 9:534–540.
- 714 Pereira S.P., J.M.L. Ribeiro, A.D. Vatulescu, K. Findlay, A.J. MacDougall and P.A.P. Jackson. (2011)  
715 Extensin network formation in *Vitis vinifera* callus cells is an essential and causal event in rapid  
716 and H<sub>2</sub>O<sub>2</sub>-induced reduction in primary cell wall hydration. *BMC Plant Biology* 11:106-121.
- 717 Price, N.J., Pinheiro, C., Soares, C.M., Ashford, D.A., Ricardo, C.P., and Jackson, P.A. (2003). A  
718 biochemical and molecular characterization of LEP1, an extensin peroxidase from lupin. *J. Biol.*  
719 *Chem.* 278:41389–41399.
- 720 Ringli C. (2010). The hydroxyproline-rich glycoprotein domain of the Arabidopsis LRX1 requires Tyr for  
721 function but not for insolubilization in the cell wall. *Plant J.* 63, 662–669.
- 722 Rodrigues, O. et al. (2017). Aquaporins facilitate hydrogen peroxide entry into guard cells to mediate  
723 ABA- and pathogen-triggered stomatal closure. *Proc Natl Acad Sci USA* 114, 9200-9205,  
724 doi:10.1073/pnas.1704754114.



- 725 Saito, F., Suyama, A., Oka, T., Yoko-o, T., Matsuoka, K., Jigami, Y., and Shimma, Y. (2014). Identification  
726 of novel peptidyl serine O-galactosyltransferase gene family in plants. *J. Biol. Chem.* 30:20405–  
727 20420.
- 728 Saitou N, Nei M. (1987). The neighbor-joining method: a new method for reconstruction of  
729 phylogenetic trees. *Mol Biol Evol*4:406–25.
- 730 Šali A., and Tom L Blundell. (1993). Comparative protein modelling by satisfaction of spatial restraints.  
731 *J. of Molecular biology*, 234(3):779–815.
- 732 Savelli B., Li Q., Webber M., Jemmat A.M., Robitaille A., Zamocky M., Mathe C., Dunand C. (2019).  
733 RedoxiBase a database for ROS homeostasis regulated proteins. *Redox Biol.*  
734 doi.org/10.1016/j.redox.2019.101247.
- 735 Schnabelrauch, L.S., Kieliszewski, M., Upham, B.L., Alizedeh, H., and Lamport, D. (1996). Isolation of  
736 pl 4.6 extensin peroxidase from tomato cell suspension cultures and identification of Val-Tyr-Lys  
737 as putative intermolecular cross-link site. *Plant J.* 9:477–489.
- 738 Sede, A.R., Borassi, C., Wengier, D.L., Mecchia, M.A., Estevez, J.M., and Muschiatti, J.P. (2018).  
739 Arabidopsis pollen extensins LRX are required for cell wall integrity during pollen tube growth.  
740 *FEBS Lett.* 592, 233–243.
- 741 Shen Y., Rosendale M., Campbell R.E., D. Perrais (2014). pHuji, apH-sensitive red fluorescent protein  
742 for imaging of exo- and endocytosis. *J. Cell Biol.* 207 (3):419-432.
- 743 Smith, A.T., Santama, N., Dacey, S., Edwards, M., Bray, R.C., Thorneley, R.N., and Burke, J.F. (1990).  
744 Expression of a synthetic gene for horseradish peroxidase C in *Escherichia coli* and folding and  
745 activation of the recombinant enzyme with Ca<sup>2+</sup> and heme. *J. Biol. Chem.* 265: 13335–13343.
- 746 Stafstrom, J.P., and Staehelin, L.A. (1986). The role of carbohydrate in maintaining extensin in an  
747 extended conformation. *Plant Physiol.* 81:242-246.
- 748 Stoddard, A and Rolland, V. (2018). I see the light!. Fluorescent proteins suitable for the cell  
749 wall/apoplast targeting in *Nicotiana benthamiana* leaves. *Plant Direct.* doi.org/10.1002/pld3.112
- 750 Strasser, R. (2016). Plant protein glycosylation. *Glycobiology.* 26(9):926–939.
- 751 Stratford, S., et al. (2001). A leucine-rich repeat region is conserved in pollen extensin-like (Pex)  
752 proteins in monocots and dicots. *Plant Mol. Biol.* 46:43–56.
- 753 Takeda S, et al. (2008) Local positive feedback regulation determines cell shape in root hair cells.  
754 *Science* 319:1241–1244.
- 755 Trott O., and Arthur J Olson. (2010). Autodock vina: improving the speed and accuracy of docking with  
756 a new scoring function, efficient optimization, and multithreading. *Journal of Computational*  
757 *Chem.* 31(2):455–461.
- 758 Vanacore R, Ham AJ, Voehler M, Sanders CR, Conrads TP, Veenstra TD, Sharpless KB, Dawson PE,  
759 Hudson BG (2009) A sulfilimine bond identified in collagen IV. *Science* 325:1230–1234.
- 760 Velasquez, S.M., Ricardi, M.M., Dorosz, J.G., Fernandez, P.V., Nadra, A.D., Pol-Fachin, L., Egelund, J.,  
761 Gille, S., Ciancia, M., Verli, H., et al. (2011). O-glycosylated cell wall extensins are essential in root  
762 hair growth. *Science* 332:1401–1403.
- 763 Velasquez M, Salter JS, Dorosz JG, Petersen BL, Estevez JM. (2012). Recent advances on the  
764 posttranslational modifications of EXTs and their roles in plant cell walls. *Frontiers in plant science*  
765 3, 93.

- 766 Velasquez SM, Marzol E, Borassi C, Pol-Fachin L, Ricardi MM, Mangano S, Denita JS, Salgado SJ,  
767 Gloazzo DJ, Marcus SE. (2015a). Low sugar is not always good: Impact of specific O-glycan defects  
768 on tip growth in Arabidopsis. *Plant Physiology* 168, 808–813.
- 769 Velasquez, S.M., Ricardi, M.M., Poulsen, C.P., Oikawa, A., Dilokpimol, A., Halim, A., Mangano, S.,  
770 Denita-Juarez, S.P., Marzol, E., Salgoda Salter, J.D., et al. (2015b). Complex regulation of prolyl-4-  
771 hydroxylases impacts root hair expansion. *Mol. Plant* 8:734–746.
- 772 Wang, X., Wang, K., Yin, G., Liu, X., Liu, M., Cao, N., Duan, Y., Gao, H., Wang, W., Ge, W., et al. (2018).  
773 Pollen-expressed leucine-rich repeat extensins are essential for pollen germination and growth.  
774 *Plant Physiol.* 176, 1993–2006.
- 775 Wojtaszek, P., Trethowan, J., and Bolwell, G.P. (1997). Reconstitution in vitro of the components and  
776 conditions required for the oxidative cross-linking of extracellular proteins in French bean  
777 (*Phaseolus vulgaris* L.). *FEBS Lett.* 405:95–98.
- 778 Yi K, Menand B, Bell E, Dolan L. (2010). A basic helix-loop-helix transcription factor controls cell growth  
779 and size in root hairs. *Nature genetics* 43: 264-267.



780

781

782 **Figure 1. Characterization of root hair-specific PRX01, PRX44 and PRX73 expression and mutant**  
 783 **analysis.**

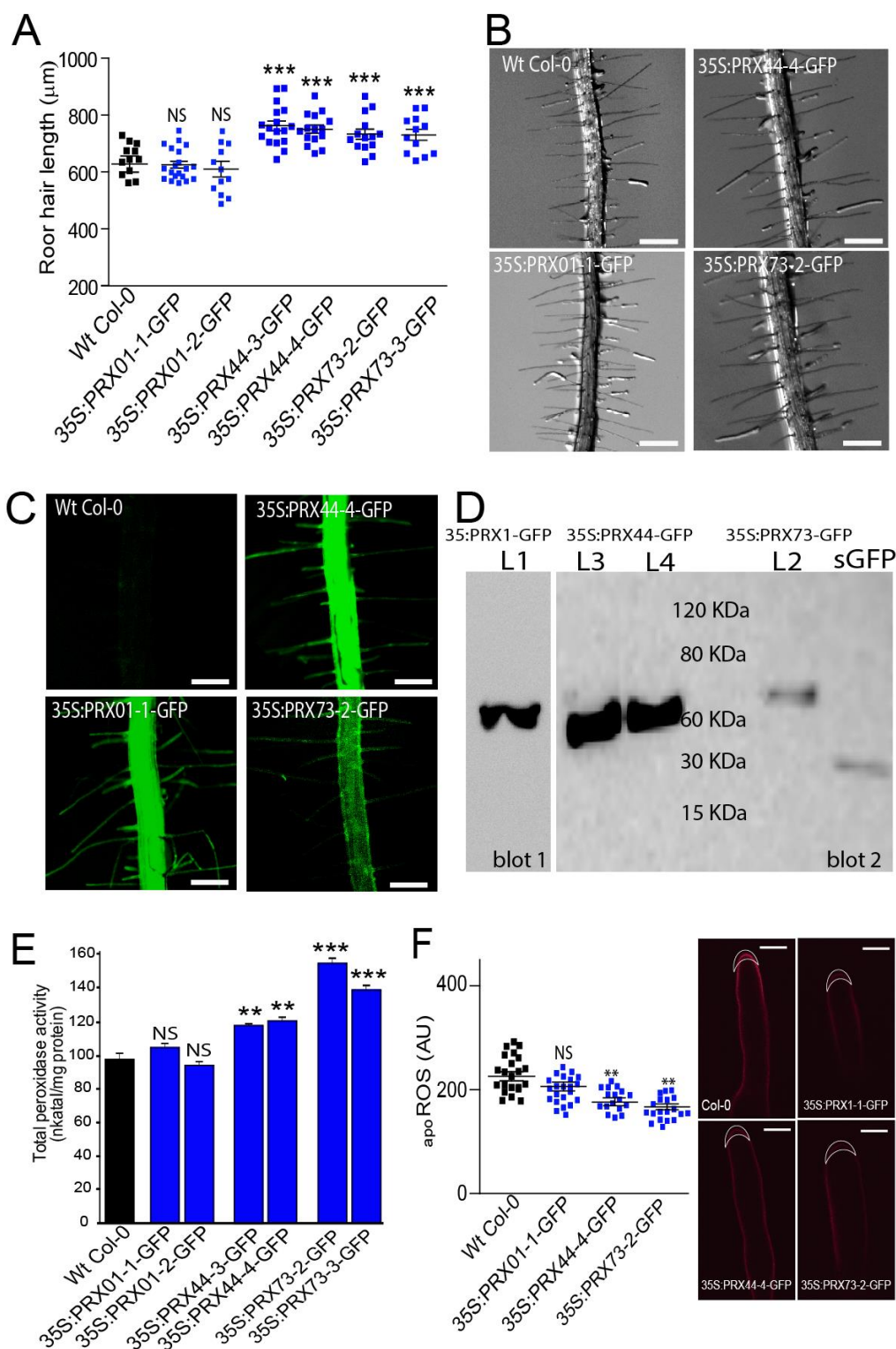
784 **(A)** GFP-tagged transcriptional reporters of PRX01, PRX44 and PRX73 show expression in the root  
785 elongation zone and specifically in root hairs (bottom). Scale bar = 20  $\mu$ m. (\*) indicates atrichoblast  
786 cell layers, which lack GFP expression.

787 **(B)** Root hair length phenotype of Wt and the *prx01,44,73* triple mutant. Left, box-plot of root hair  
788 length. Horizontal lines show the means. P-value determined by one-way ANOVA, (\*\*\*)  $P < 0.001$ .  
789 Right, bright-field images exemplifying the root hair phenotype in each genotype. Scale bars, 1 mm.

790 **(C)** Peroxidase activity in Wt and *prx01,44,73* triple mutant roots. Enzyme activity values (expressed  
791 as nkatal/mg protein) are shown as the mean of three replicates  $\pm$  SD. P-value determined by one-  
792 way ANOVA, (\*\*\*)  $P < 0.001$ .

793 **(D)** Cytoplasmic ROS levels measured with H<sub>2</sub>DCF-DA in Wt and *prx01,44,73* triple mutant root hairs.  
794 Horizontal lines show the means. P-values determined by one-way ANOVA, (\*\*\*)  $P < 0.001$  and (\*\*)  
795  $P < 0.01$ .

796 **(E)** Apoplastic ROS levels measured with Amplex™ UltraRed (AUR) in Wt and *prx01,44,73* triple  
797 mutant root hairs. ROS signal was quantified from the root hair cell tip. Left, box-plot of apoROS  
798 values. Horizontal lines show the means. P-value determined by one-way ANOVA, (\*\*\*)  $P < 0.001$ .  
799 Right, fluorescence images exemplifying apoROS detection in root hair apoplast.



800  
801

802 **Figure 2. Over-expression of PRX44 and PRX73 promotes root hair growth and higher root**  
803 **peroxidase activity.**

804 **(A)** Root hair length phenotype of Wt and PRX<sup>OE</sup> lines (in Wt background). Box-plot of root hair length.  
805 Horizontal lines show the means. P-values determined by one-way ANOVA, (\*\*\*) P<0.001, (NS) not  
806 significantly different.

807 **(B)** Bright-field images exemplifying the root hair phenotype analyzed in Figure 2A. Scale bar = 0.5  
808 mm.

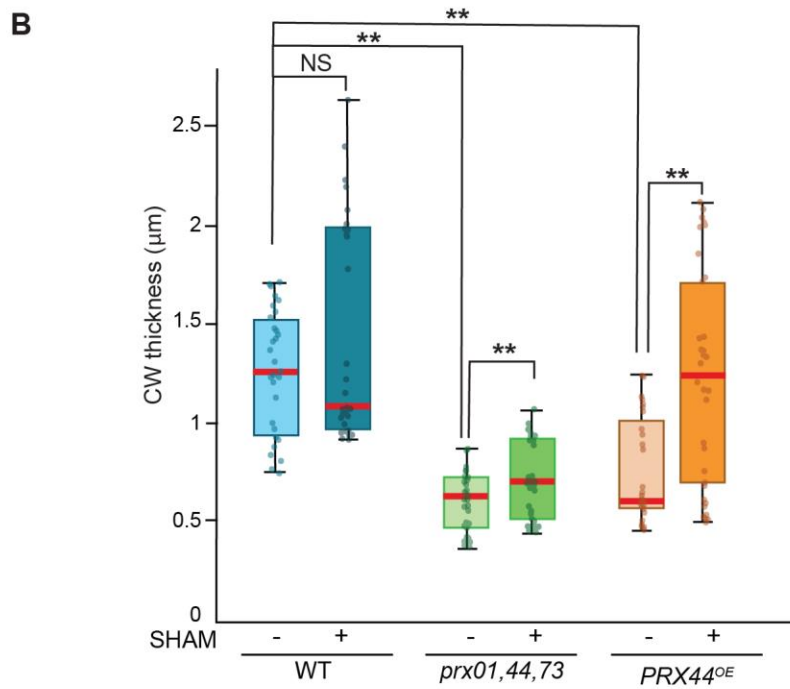
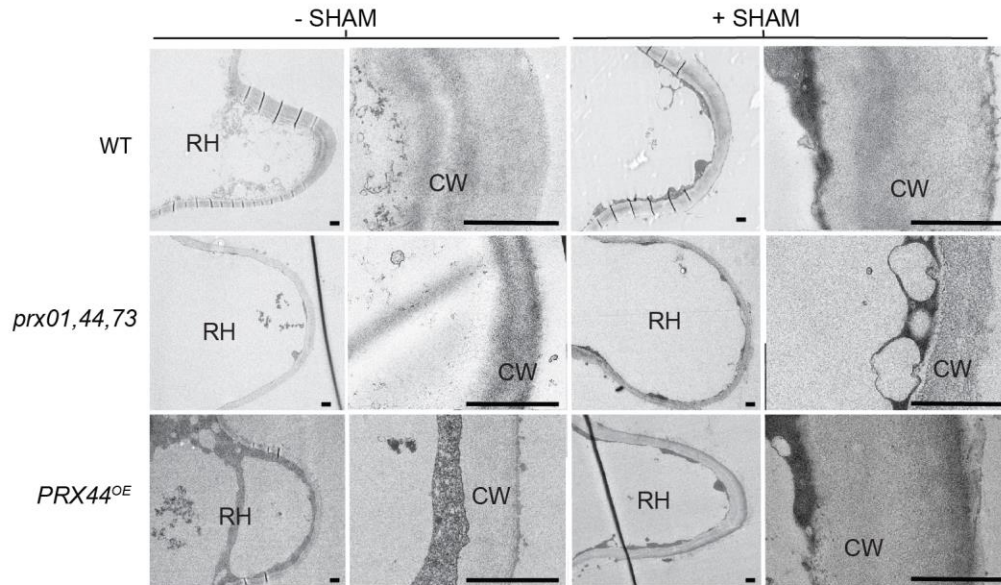
809 **(C)** Expression of GFP-tagged 35S:PRX01, 35S:PRX44 and 35S:PRX73 in root hair cells.

810 **(D)** Western blot of PRX01-GFP, PRX44-GFP and PRX73-GFP. Soluble GFP (sGFP) was used as control.  
811 The predicted molecular weights are 62.6 KDa for PRX01-GFP, 60.8 KDa for PRX44-GFP, 62.9 KDa for  
812 PRX73 and 27 KDa for sGFP.

813 **(E)** Assays of total peroxidase activity in Wt and PRXs<sup>OE</sup> lines (in Wt background). Enzyme activity  
814 (expressed in nkatal/mg protein) was determined by a guaiacol oxidation-based assay. Values are the  
815 mean of three replicates ± SD. P-values determined by one-way ANOVA, (\*\*\*) P<0.001, (\*\*) P<0.01,  
816 (NS) not significantly different.

817 **(F)** Apoplastic ROS levels measured with Amplex™ UltraRed (AUR) in Wt and PRX<sup>OE</sup> lines (in Wt  
818 background). ROS signal was quantified from the root hair cell tip. Left, box plot of apoROS values.  
819 Horizontal lines show the means. P-values determined by one-way ANOVA, (\*\*) P<0.01, (NS) not  
820 significantly different. Right, fluorescence images exemplifying apoROS detection in root hair  
821 apoplast. Scale bar = 10 µm.



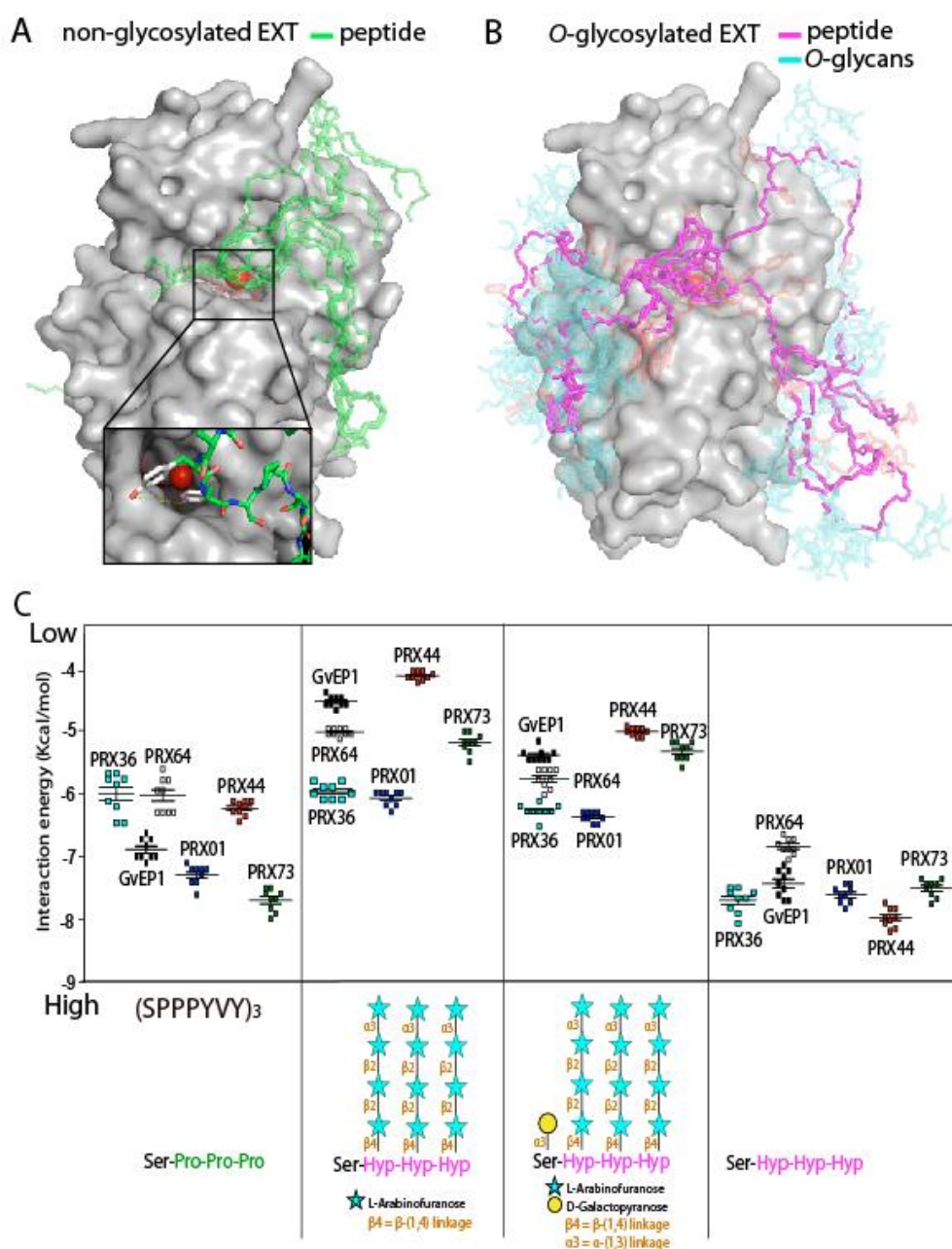




823 **Figure 3. Effect of PRX expression on cell wall thickness in root hair tips.**

824 **(A)** Transmission electron micrographs of root hair tips from *Wt*, *prx1,44,73* triple mutant, and  
825 *PRX44<sup>OE</sup>* with (+) and without (-) peroxidase inhibitor SHAM. For each genotype and treatment, a  
826 representative overview of a root hair (RH) and a detail of the cell wall at the root hair tip (CW) is  
827 shown. Scale bar = 1  $\mu$ m.

828 **(B)** Box and whisker plot showing cell wall thickness measured at the root hair tip of the three  
829 genotypes with or without SHAM treatment. (\*\*)  $P < 0.001$  determined by t-test. (NS) not significantly  
830 different.



831

832

833 **Figure 4. Interaction by an *in silico* docking approach of PRX01, PRX44 and PRX73 with EXT peptides.**

834 **(A,B)** Ten docking results for each EXT O-glycosylation state are shown superimposed on the PRX44  
835 protein surface to evaluate the consistence of docking sites.

836 **(A)** Model of PRX44 (protein surface shown in gray) complexed to a non-O-glycosylated EXT substrate  
837 (SPPPYVY)<sub>3</sub> (in green, depicted as sticks). Heme is depicted as thin sticks while iron is a red sphere.  
838 Bottom inset, two close tyrosine residues dock near to the possible active site of PRX44.

839 **(B)** Model of PRX44 (protein surface shown in gray) complexed to an O-glycosylated-EXT substrate  
840 (protein backbone shown in magenta, and O-glycans shown in light blue, both depicted as sticks).

841 Heme is depicted as thin sticks while iron is a red sphere. Arabino-galactosylated EXT peptide =  
842 [(SOOOYVY)<sub>3</sub>-AG].  
843 (C) Comparison of the binding energy of different peroxidases to EXT substrates with different degrees  
844 of *O*-glycosylation. A non-hydroxylated EXT peptide (SPPPYVY)<sub>3</sub>, a hydroxylated but not *O*-  
845 glycosylated EXT peptide [(SOOOYVY)<sub>3</sub>; O=hydroxyproline], only arabinosylated EXT-peptide  
846 [(SOOOYVY)<sub>3</sub>-A], and arabino-galactosylated EXT peptide [(SOOOYVY)<sub>3</sub>-AG] were analyzed.

847 **Table 1.** Peptidyl-Tyr and iso-dityrosine (IDT) contents in cell walls isolated from Wt, *prx01,44,73* triple  
 848 mutant, PRX<sup>OE</sup> lines and mutant lines with under-glycosylated EXTs. P-values were determined by one-  
 849 way ANOVA, (\*\*\*) P<0.001, (\*\*) P<0.01. STD=Standard Deviation. Values significantly different than  
 850 Wt are highlighted in blue if higher and in light blue if lower than Wt Col-0.  
 851

	ng Tyr/ $\mu$ g CW (STD)	ng IDT/ $\mu$ g CW (STD)
Wt Col-0	7.799 $\pm$ 0.26	0.853 $\pm$ 0.08
<i>prx01 prx44 prx73</i>	9.588 $\pm$ 0.31**	0.963 $\pm$ 0.02
PRX44 <sup>OE</sup>	8.649 $\pm$ 0.07	0.953 $\pm$ 0.04
PRX73 <sup>OE</sup>	8.700 $\pm$ 0.12	1.042 $\pm$ 0.02**
<i>under O-glycosylated EXTs</i>		
<i>sergt1-1 rra3</i>	3.530 $\pm$ 0.08***	0.235 $\pm$ 0.01***
<i>p4h5 sergt1-1</i>	3.766 $\pm$ 0.06***	0.225 $\pm$ 0.02***

852